Available online at www.sciencedirect.com
ScienceDirect
Journal of Computational Physics 219 (2006) 733–748
JOURNAL OF COMPUTATIONAL PHYSICS
www.elsevier.com/locate/jcp

Accurate calculation of Green's function of the Schrödinger equation in a block layered potential

Sihong Shao [a], Wei Cai [b,*], Huazhong Tang [a]

[a] *LMAM, School of Mathematical Sciences, Peking University, Beijing 100871, PR China*
[b] *Department of Mathematics and Statistics, University of North Carolina at Charlotte, Fretwell 390G, Charlotte, NC 28223, USA*

Received 31 October 2005; received in revised form 3 April 2006; accepted 17 April 2006
Available online 9 June 2006

Abstract

In this paper a new algorithm is presented for calculating the Green's function of the Schrödinger equation in the presence of block layered potentials. Such Green's functions have various and practical applications in quantum modelling of electron transport within nano-MOSFET transistors. The proposed method is based on expansions of the eigenfunctions of the subordinate Sturm–Liouville problems and a collocation matching procedure along possibly curved interfaces of the potential blocks. Accurate numerical results are provided to validate the proposed algorithm.

MSC: 81Q05; 34L10

Keywords: Green's function; The Schrödinger equation; Eigenfunction expansion; Sturm–Liouville problem; Block layered media

1. Introduction

Wave scattering in inhomogeneous media has various applications in engineering and physics – such as electromagnetic wave scattering in layered media, and electron density waves in variable potential fields. To simulate the wave phenomenon in such inhomogeneous media, the integral equation method is one of several popular numerical methods, together with the finite difference time domain (FDTD) method [1], the finite element (FE) method [2], and the discontinuous Galerkin time domain (DGTD) method [3]. The integral equation method is particularly useful for solving problems in unbounded domains, and yields well conditioned discrete algebraic systems. Key to the integral equation method is the existence and construction of the appropriate Green's function, which is closely related to the material properties of the background media in which the scattering centers are embedded. There are numerous studies of Green's functions in layered media, together with associated numerical algorithms for calculating their approximations [4–7]. The problem of the Green's function in layered media, stacked along the z-direction, often reduces to calculating Hankel transforms of the spectral form of the Green's function – itself defined by Fourier transforms in the horizontal,

* Corresponding author. Tel.: +1 704 687 4581; fax: +1 704 687 6415.
E-mail addresses: shaosihong@pku.edu.cn (S. Shao), wcai@uncc.edu (W. Cai), hztang@math.pku.edu.cn (H. Tang).

0021-9991/$ - see front matter
doi:10.1016/j.jcp.2006.04.009

x- and y-, dimensions. However, in the case of the electron density in a MOSFET device, the background potentials – created by the source and drain and the substrate – are not constant along the horizontal directions and must be modelled by block constants at least. Since the potentials are part of the linear operator in the Schrödinger equation, the Fourier transform approach cannot be used in this case.

In this paper, a new method is proposed for calculating the Green's function of the two-dimensional Schrödinger equation in the presence of block layered potentials. The Schrödinger operator is assumed to be separable in the presence of such potentials. The overall procedure occurs in two steps. Firstly, we represent the Green's function by means of separating the Schrödinger operator into vertical and horizontal components. An infinite sequence of eigenfunctions is generated from the vertical equation while the coefficients for the corresponding infinite series expansion are obtained by solving the horizontal equation. The eigenfunctions can be pre-calculated using one-dimensional Sturm–Liouville eigenvalue-problem solvers for piecewise constant coefficients. Secondly, the continuity conditions of the Green's function along the potential block boundaries via a collocation method is used to determine the coefficients in the eigenfunction expansions of the first step.

Some previous work on the Green's function for Maxwell's equations in layered media can be found in [4–6]. The work in [4] for layered media covered the case where the material constants are the same for each horizontal layer. In [5,6], blocked layered media is considered where more than one material constant is allowed for each horizontal layer. However, a different approach is used to construct the solution there. Though, both our approach and the approach in [5,6] have employed eigenfunctions of the split operators, we have used an eigenfunction expansion for the singular source to obtain differential equations for the expansion coefficients of the Green's function. Moreover, a collocation method based on Gauss points is used in this paper to obtain remaining unknown coefficients, and we also address a more general case in this paper where the interface between material blocks is curved.

Numerical examples, given in Section 4, validate the algorithm and demonstrate good convergence with respect to truncation in the eigenfunction series expansion. The rest of the paper is organized as follows: in Section 2, the mathematical model is described; in Section 3, the algorithm for calculating the Green's function is given in detail; and in Section 5, a conclusion, together with a discussion of future research issues, is presented.

2. Retarded Green's function in block layered potentials

The motivation for studying the Green's function of the Schrödinger equation in block layered potentials comes from the investigation of electron transport in nano-MOSFET transistors where the drift-diffusion equation fails to describe the electron transport through the nano-scale inversion layers [8]. The fact that the potential within an horizontal layer is not constant is a result of the potential difference in the source and drain regions. The Green's function is the key component in the generalized Landauer–Büttiker formula in calculating electron transport properties [12]. Moreover, other scenarios can also arise that we will encounter Green's functions for block layered media such as the scattering of underwater objects near coastlines.

Given an infinite strip domain Ω_L (see Fig. 1), let $\Gamma_i = \{(x(t), y(t)) : t \in [0,1]\}$ denote the curved interface, and Γ_t (Γ_b) the top (bottom) boundary of Ω_L. Meanwhile, we let Ω_L^l (Ω_L^r) denote the sub-domain to the left (right) of Γ_i.

We define a retarded Green's function $g_L(\boldsymbol{r};\boldsymbol{r}^*, E)$ for the Schrödinger equation, $\boldsymbol{r} = (x, y)$ and $\boldsymbol{r}^* = (x^*, y^*)$ in the infinite strip domain Ω_L, with block constant potential $V_L(\boldsymbol{r})$ as solution to the following equation:

$$\left[E + \frac{\hbar^2}{2}\nabla\left(\frac{1}{m(\boldsymbol{r})}\nabla\right) - V_L(\boldsymbol{r})\right] g_L(\boldsymbol{r};\boldsymbol{r}^*, E) = \delta(\boldsymbol{r} - \boldsymbol{r}^*), \quad \boldsymbol{r}, \boldsymbol{r}^* \in \Omega_L, \tag{1}$$

where the potential $V_L(\boldsymbol{r})$ is of the following form:

$$V_L(\boldsymbol{r}) = \begin{cases} V_k^l, & \boldsymbol{r} \in \Omega_L^l \cap \{(x,y) : x \in \mathbb{R}, y \in [d_{k-1}, d_k]\}, \\ V_k^r, & \boldsymbol{r} \in \Omega_L^r \cap \{(x,y) : x \in \mathbb{R}, y \in [d_{k-1}, d_k]\}, \end{cases} \quad (k = 1, \ldots, N), \tag{2}$$

and V_k^l and V_k^r are different constants, and the effective mass $m(\boldsymbol{r})$ is assumed to be piecewise constant as in the form of $V_L(\boldsymbol{r})$, and $\delta(\boldsymbol{r})$ is the Dirac delta function. Here E is the electron energy and $\hbar = h/2\pi$ with h is the Planck's constant. In many cases, we will simply write Green's function as $g_L(\boldsymbol{r};\boldsymbol{r}^*)$.

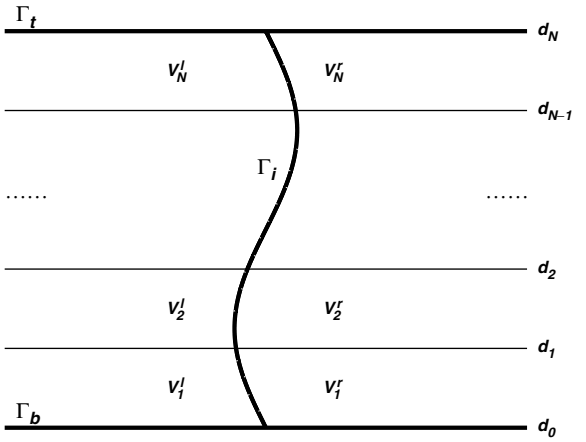

Fig. 1. Ω_L: geometry for the block layered potentials.

- *Boundary conditions*. We will assume zero Dirichlet boundary conditions on the top and bottom boundaries of Ω_L: $g_L(\boldsymbol{r};\boldsymbol{r}^*) = 0$, if $\boldsymbol{r} \in \Gamma_t$ or Γ_b. For $x \to \pm\infty$, a Sommerfeld outgoing radiation condition is assumed

$$(\pm\partial_x - ik)g_L(\boldsymbol{r};\boldsymbol{r}^*) \to 0, \quad x \to \pm\infty, \tag{3}$$

where $k = \sqrt{\frac{2m(E-V_L)}{\hbar^2}}$.

3. Algorithm for calculating Green's function $g_L(\boldsymbol{r};\boldsymbol{r}^*)$

The Green's function $g_L(\boldsymbol{r};\boldsymbol{r}^*)$ defined above will be represented by eigenfunction expansions for regions $\boldsymbol{r} \in \Omega_L^{\mathrm{r}}$ and $\boldsymbol{r} \in \Omega_L^{\mathrm{l}}$, respectively, and the continuity conditions due to the normal continuity of the current operator $J = \frac{\hbar q}{m}\mathrm{Im}[(\nabla g_L)^* g_L]$[12] will be enforced at the interface Γ_{i}, for every $\boldsymbol{r}_\Gamma = (x(t_\Gamma), y(t_\Gamma)) := (x_\Gamma, y_\Gamma) \in \Gamma_{\mathrm{i}}$,

$$\begin{aligned} &g_L(\boldsymbol{r}_\Gamma+;\boldsymbol{r}^*) = g_L(\boldsymbol{r}_\Gamma-;\boldsymbol{r}^*), \\ &\frac{1}{m+}\frac{\partial g_L(\boldsymbol{r}_\Gamma+;\boldsymbol{r}^*)}{\partial \boldsymbol{n}_\Gamma} = \frac{1}{m-}\frac{\partial g_L(\boldsymbol{r}_\Gamma-;\boldsymbol{r}^*)}{\partial \boldsymbol{n}_\Gamma}, \end{aligned} \tag{4}$$

where $+$ $(-)$ after m or $\boldsymbol{r}_\Gamma$ represents taking the limit from the right (left) of the curved interface $\Gamma_{\mathbf{i}}$, and $\boldsymbol{n}_\Gamma$ is the right-pointing normal of the interface Γ_{i}.

The construction of $g_L(\boldsymbol{r};\boldsymbol{r}^*)$ will be done in three steps. Firstly, we will define two sets of eigenfunctions $\{\psi_p^{\mathrm{l}}(y)\}_{p=1}^{\infty}$ and $\{\psi_p^{\mathrm{r}}(y)\}_{p=1}^{\infty}$, along the vertical y-direction based on the piecewise constants V_k^{l} and V_k^{r}, respectively. Secondly, we expand the Green's function in terms of those eigenfunctions with x-variable coefficients $c_p^{\mathrm{l}}(x,x^*,y^*)$ and $c_p^{\mathrm{r}}(x,x^*,y^*)$, and then find the differential equations and the general solutions for $c_p^{\mathrm{l,r}}(x,x^*,y^*)$. Thirdly, we use the continuity conditions (4) to determine the remaining constants in the general expressions of $c_p^{\mathrm{l,r}}(x,x^*,y^*)$.

- *Step 1*: *Eigenfunctions* $\psi_p(y)$. Define orthogonal eigenfunctions $\psi_p(y)$ for the differential operator

$$\begin{aligned} &\left[\frac{\hbar^2}{2}\frac{\mathrm{d}}{\mathrm{d}y}\left(\frac{1}{m}\frac{\mathrm{d}}{\mathrm{d}y}\right) - V_L(y)\right]\psi_p(y) = -\lambda_p\psi_p(y), \quad d_0 \leqslant y \leqslant d_N, \\ &\psi_p(d_0) = \psi_p(d_N) = 0, \end{aligned} \tag{5}$$

where $1 \leqslant p < \infty$. Due to the self-adjointness of the differential operator, it is known [9,10] that the eigenfunctions $\{\psi_p(y)\}_{p=1}^{\infty}$ form a complete and orthogonal basis for $L^2[d_0, d_N]$. Thus, in distribution sense, we can expand the Dirac delta function in terms of these eigenfunctions

$$\delta(y-y^*)=\sum_{p=1}^{\infty}\psi_p(y)\psi_p(y^*). \tag{6}$$

For each set of the constants $\{V_k^{\mathrm{l}}\}_{k=1}^N$ and $\{V_k^{\mathrm{r}}\}_{k=1}^N$, the resulting eigenfunctions obtained will be denoted as $\{\psi_p^{\mathrm{l}}(y)\}_{p=1}^{\infty}$ and $\{\psi_p^{\mathrm{r}}(y)\}_{p=1}^{\infty}$, respectively.The eigenvalues and eigenfunctions of the Sturm–Liouville problem (5) can be obtained by a Pruess method (see Appendix A), designed specifically for finding numerical solutions of Sturm–Liouville problems with piecewise constant coefficients as in (5). A key component in the Pruess method is a stabilized shooting algorithm for computing the approximate eigenvalues, while the integrations are preformed analytically.

- *Step 2*: *Eigenfunction expansions*. Consider the case when $\boldsymbol{r}^*\in\Omega_L^{\mathrm{r}}$ (the case of $\boldsymbol{r}^*\in\Omega_L^{\mathrm{l}}$ can be handled similarly). We now expand $g_L(\boldsymbol{r};\boldsymbol{r}^*)$ using the eigenfunctions $\psi_p^{\mathrm{l,r}}(y)$ of step 1:

$$g_L^{\mathrm{r}}(\boldsymbol{r};\boldsymbol{r}^*)=\sum_{p=1}^{\infty}c_p^{\mathrm{r}}(x,x^*,y^*)\psi_p^{\mathrm{r}}(y)\psi_p^{\mathrm{r}}(y^*),\quad \boldsymbol{r}\in\Omega_L^{\mathrm{r}}, \tag{7}$$

$$g_L^{\mathrm{l}}(\boldsymbol{r};\boldsymbol{r}^*)=\sum_{p=1}^{\infty}c_p^{\mathrm{l}}(x,x^*,y^*)\psi_p^{\mathrm{l}}(y)\psi_p^{\mathrm{l}}(y^*),\quad \boldsymbol{r}\in\Omega_L^{\mathrm{l}}. \tag{8}$$

Next, we will determine the differential equations for the variable coefficients $c_p^{\mathrm{l,r}}(x,x^*,y^*)$ by inserting Eqs. (7) and (8) into Eq. (1).

Case 1 ($\boldsymbol{r}\in\Omega_L^{\mathrm{r}}$). Substituting (7) into (1) and using (5) and (6), we get an inhomogeneous equation

$$\left[E+\frac{\hbar^2}{2}\frac{\mathrm{d}}{\mathrm{d}x}\left(\frac{1}{m^{\mathrm{r}}}\frac{\mathrm{d}}{\mathrm{d}x}\right)-\lambda_p^{\mathrm{r}}\right]c_p^{\mathrm{r}}(x,x^*,y^*)=\delta(x-x^*), \tag{9}$$

the solution of which can be expressed

$$c_p^{\mathrm{r}}(x,x^*,y^*)=\begin{cases}A_{1,p}^-\exp[-\mathrm{i}k_p^{\mathrm{r}}(x-x^*)]+A_{2,p}^-\exp[\mathrm{i}k_p^{\mathrm{r}}(x-x^*)], & x<x^*,\\ A_p^+\exp[\mathrm{i}k_p^{\mathrm{r}}(x-x^*)], & x>x^*,\end{cases} \tag{10}$$

where $k_p^{\mathrm{r}}=\sqrt{\frac{2m^{\mathrm{r}}(E-\lambda_p^{\mathrm{r}})}{\hbar^2}}$. For $x>x^*$, we have used the Sommerfeld radiation condition (3) to retain only the right-going wave.

Differentiating Eq. (10) with respect to x, we have

$$\frac{\mathrm{d}c_p^{\mathrm{r}}(x,x^*,y^*)}{\mathrm{d}x}=\begin{cases}-\mathrm{i}k_p^{\mathrm{r}}A_{1,p}^-\exp[-\mathrm{i}k_p^{\mathrm{r}}(x-x')]+\mathrm{i}k_p^{\mathrm{r}}A_{2,p}^-\exp[\mathrm{i}k_p^{\mathrm{r}}(x-x^*)], & x<x^*,\\ \mathrm{i}k_p^{\mathrm{r}}A_p^+\exp[\mathrm{i}k_p^{\mathrm{r}}(x-x^*)], & x>x^*.\end{cases} \tag{11}$$

The function $c_p^{\mathrm{r}}(x,x^*,y^*)$ must be continuous and its derivative has a jump of $\frac{2m^{\mathrm{r}}}{\hbar^2}$ at $x=x^*$, namely,

$$c_p^{\mathrm{r}}(x^*+,x^*,y^*)=c_p^{\mathrm{r}}(x^*-,x',y^*)\Rightarrow A_p^+-A_{1,p}^--A_{2,p}^-=0, \tag{12}$$

$$\frac{\mathrm{d}c_p^{\mathrm{r}}(x^*+,x^*,y^*)}{\mathrm{d}x}-\frac{\mathrm{d}c_p^{\mathrm{r}}(x^*-,x^*,y^*)}{\mathrm{d}x}=\frac{2m^{\mathrm{r}}}{\hbar^2}\Rightarrow A_p^++A_{1,p}^--A_{2,p}^-=\gamma_p^{\mathrm{r}}, \tag{13}$$

where

$$\gamma_p^{\mathrm{r}}=\frac{2m^{\mathrm{r}}}{\mathrm{i}k_p^{\mathrm{r}}\hbar^2}. \tag{14}$$

From (12) and (13), we have

$$\begin{aligned}A_{1,p}^-&=\frac{\gamma_p^{\mathrm{r}}}{2},\\ A_{2,p}^-&=A_p^+-\frac{\gamma_p^{\mathrm{r}}}{2}.\end{aligned} \tag{15}$$

Case 2 ($\boldsymbol{r} \in \Omega_L^{\mathrm{l}}$). Substituting (8) into (1) and using (5), we obtain the following homogeneous equation:

$$\left[E + \frac{\hbar^2}{2}\frac{\mathrm{d}}{\mathrm{d}x}\left(\frac{1}{m^{\mathrm{l}}}\frac{\mathrm{d}}{\mathrm{d}x}\right) - \lambda_p^{\mathrm{l}}\right] c_p^{\mathrm{l}}(x, x^*, y^*) = 0. \tag{16}$$

For the retarded Green's function, $c_p^{\mathrm{l}}(x, x^*, y^*)$ will have the following left-going wave form, observing the Sommerfeld radiation condition (3),

$$c_p^{\mathrm{l}}(x, x^*, y^*) = B_p^- \exp[-\mathrm{i}k_p^{\mathrm{l}}(x - x^*)], \tag{17}$$

where $k_p^{\mathrm{l}} = \sqrt{\frac{2m^{\mathrm{l}}(E-\lambda_p^{\mathrm{l}})}{\hbar^2}}$.

- *Step 3*: *Interface matching at* $\boldsymbol{r}_\Gamma = (x_\Gamma, y_\Gamma) \in \Gamma_{\mathrm{i}}$. In order to determine the remaining constants in (10) and (17), we will enforce the continuity condition (4) for the two series expansions $g_L^{\mathrm{l}}(\boldsymbol{r}; \boldsymbol{r}^*)$ and $g_L^{\mathrm{r}}(\boldsymbol{r}; \boldsymbol{r}^*)$. After truncating the expansion to a finite order P, we arrive at the equations for unknown coefficients,

$$\begin{aligned}
&\sum_{p=1}^{P}[A_{1,p}^- \exp(-\mathrm{i}k_p^{\mathrm{r}}(x_\Gamma - x^*)) + A_{2,p}^- \exp(\mathrm{i}k_p^{\mathrm{r}}(x_\Gamma - x^*))]\psi_p^{\mathrm{r}}(y_\Gamma)\psi_p^{\mathrm{r}}(y^*) \\
&\quad = \sum_{p=1}^{P}[B_p^- \exp(-\mathrm{i}k_p^{\mathrm{l}}(x_\Gamma - x^*))]\psi_p^{\mathrm{l}}(y_\Gamma)\psi_p^{\mathrm{l}}(y^*) \\
&\frac{1}{m+}\sum_{p=1}^{P}\{y_\Gamma'[-\mathrm{i}k_p^{\mathrm{r}}A_{1,p}^- \exp(-\mathrm{i}k_p^{\mathrm{r}}(x_\Gamma - x^*)) + \mathrm{i}k_p^{\mathrm{r}}A_{2,p}^- \exp(\mathrm{i}k_p^{\mathrm{r}}(x_\Gamma - x^*))]\psi_p^{\mathrm{r}}(y_\Gamma) \\
&\qquad - x_\Gamma'[A_{1,p}^- \exp(-\mathrm{i}k_p^{\mathrm{r}}(x_\Gamma - x^*)) + A_{2,p}^- \exp(\mathrm{i}k_p^{\mathrm{r}}(x_\Gamma - x^*))](\psi_p^{\mathrm{r}})'(y_\Gamma)\}\psi_p^{\mathrm{r}}(y^*) \\
&\quad = \frac{1}{m-}\sum_{p=1}^{P}\{y_\Gamma'[-\mathrm{i}k_p^{\mathrm{l}}B_p^- \exp(-\mathrm{i}k_p^{\mathrm{l}}(x_\Gamma - x^*))]\psi_p^{\mathrm{l}}(y_\Gamma) - x_\Gamma'[B_p^- \exp(-\mathrm{i}k_p^{\mathrm{l}}(x_\Gamma - x^*))](\psi_p^{\mathrm{l}})'(y_\Gamma)\}\psi_p^{\mathrm{l}}(y^*).
\end{aligned} \tag{18}$$

where $x_\Gamma' := x'(t_\Gamma)$ and $y_\Gamma' := y'(t_\Gamma)$.

Due to (15), the following inhomogeneous system of equations for $\{A_p^+, B_p^-\}_{p=1}^P$ is obtained

$$\begin{aligned}
&\sum_{p=1}^{P}\{A_p^+ \exp(\mathrm{i}k_p^{\mathrm{r}}(x_\Gamma - x^*))\psi_p^{\mathrm{r}}(y_\Gamma)\psi_p^{\mathrm{r}}(y^*) - B_p^- \exp(-\mathrm{i}k_p^{\mathrm{l}}(x_\Gamma - x^*))\psi_p^{\mathrm{l}}(y_\Gamma)\psi_p^{\mathrm{l}}(y^*)\} = h_1(\boldsymbol{r}_\Gamma; \boldsymbol{r}^*), \\
&\sum_{p=1}^{P}\left\{\frac{1}{m+}A_p^+[y_\Gamma'\mathrm{i}k_p^{\mathrm{r}}\psi_p^{\mathrm{r}}(y_\Gamma) - x_\Gamma'(\psi_p^{\mathrm{r}})'(y_\Gamma)] \exp(\mathrm{i}k_p^{\mathrm{r}}(x_\Gamma - x^*))\psi_p^{\mathrm{r}}(y^*) + \frac{1}{m-}B_p^-[y_\Gamma'\mathrm{i}k_p^{\mathrm{l}}\psi_p^{\mathrm{l}}(y_\Gamma)\right. \\
&\qquad \left. + x_\Gamma'(\psi_p^{\mathrm{l}})'(y_\Gamma)] \exp(-\mathrm{i}k_p^{\mathrm{l}}(x_\Gamma - x^*))\psi_p^{\mathrm{l}}(y^*)\right\} = h_2(\boldsymbol{r}_\Gamma; \boldsymbol{r}^*),
\end{aligned} \tag{19}$$

where

$$\begin{aligned}
h_1(\boldsymbol{r}_\Gamma; \boldsymbol{r}^*) &= \sum_{p=1}^{P}\frac{2m+}{k_p^{\mathrm{r}}\hbar^2}\sin(k_p^{\mathrm{r}}(x_\Gamma - x^*))\psi_p^{\mathrm{r}}(y_\Gamma)\psi_p^{\mathrm{r}}(y^*), \\
h_2(\boldsymbol{r}_\Gamma; \boldsymbol{r}^*) &= \sum_{p=1}^{P}\left[\frac{2y_\Gamma'}{\hbar^2}\cos(k_p^{\mathrm{r}}(x_\Gamma - x^*))\psi_p^{\mathrm{r}}(y_\Gamma) - \frac{2x_\Gamma'}{k_p^{\mathrm{r}}\hbar^2}\sin(k_p^{\mathrm{r}}(x_\Gamma - x^*))(\psi_p^{\mathrm{r}})'(y_\Gamma)\right]\psi_p^{\mathrm{r}}(y^*).
\end{aligned} \tag{20}$$

In order to obtain $\{A_p^+, B_p^-\}_{p=1}^P$, system (19) will be collocated at pre-selected Gauss points $\{y_\Gamma = y_j\}_{j=1}^P$. From (19), we can see that the coefficients $\{A_p^+, B_p^-\}_{p=1}^P$ depend on x^*, y^*, thus $\{c_p^{\mathrm{l,r}}(x, x^*, y^*)\}_{p=1}^P$ depend on x, x^*, y^* from (10), (17). As a result, a P-term series approximation for the Green's function $g_L(\boldsymbol{r}; \boldsymbol{r}^*)$ in Ω_L is obtained, which will be denoted by $g_{L,P}(\boldsymbol{r}; \boldsymbol{r}^*)$.

4. Numerical results

This section will present several numerical results to validate the algorithm proposed in Section 3. Since the Green's function $g_L(\boldsymbol{r}; \boldsymbol{r}^*)$ is defined by

$$\mathscr{L} g_L(\boldsymbol{r};\boldsymbol{r}^*) = \delta(\boldsymbol{r}-\boldsymbol{r}^*), \tag{21}$$

where the differential operator $\mathscr{L} = E + \frac{\hbar^2}{2}\nabla(\frac{1}{m}\nabla) - V_L$, we should expect that the approximation $g_{L,P}(\boldsymbol{r};\boldsymbol{r}^*)$ to $g_L(\boldsymbol{r};\boldsymbol{r}^*)$ satisfies

$$\mathscr{L} g_{L,P}(\boldsymbol{r};\boldsymbol{r}^*) \to \delta(\boldsymbol{r}-\boldsymbol{r}^*) \quad \text{as } P \to \infty$$

in the sense of distribution.

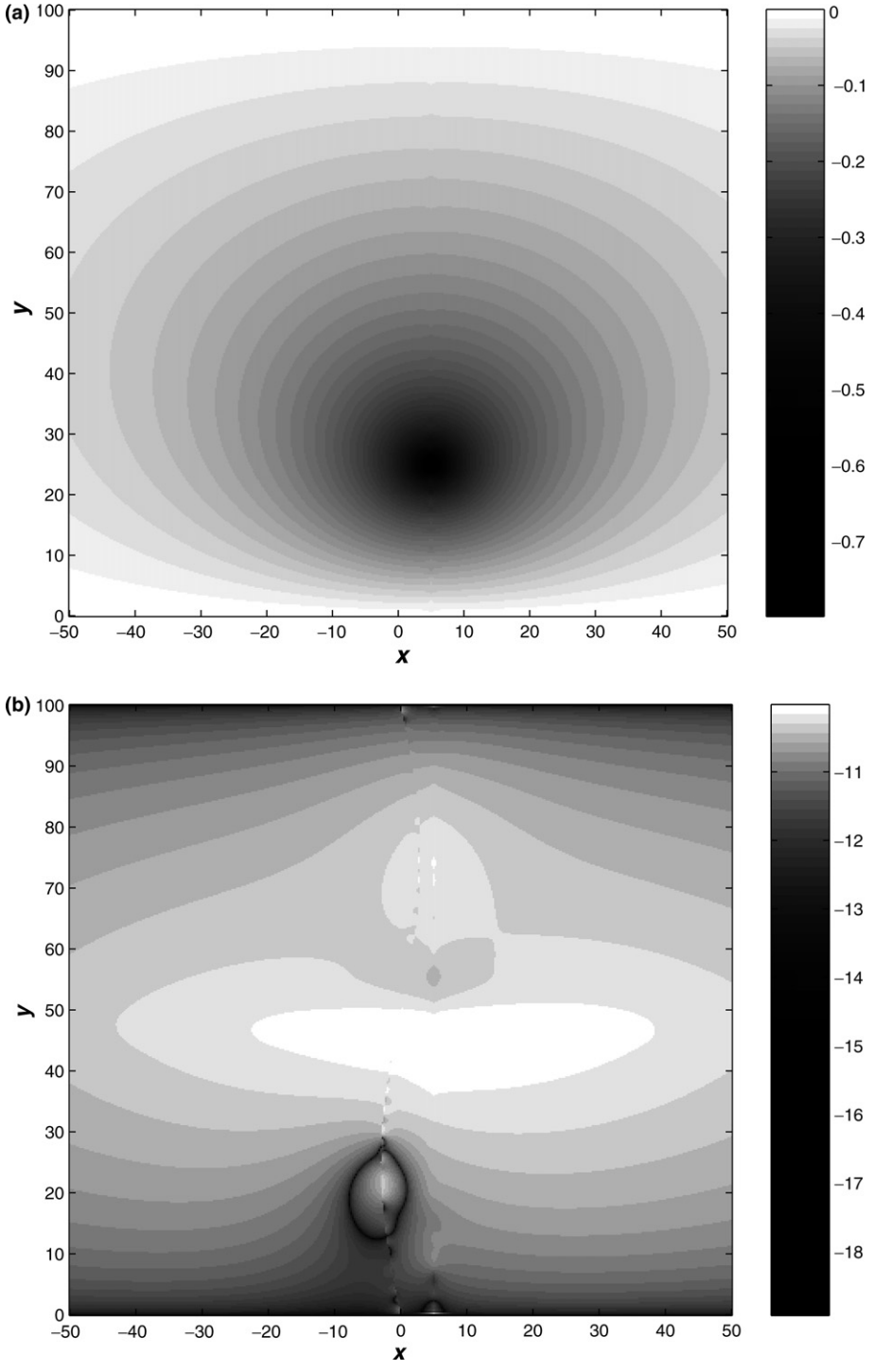

Fig. 2. Example 1: $E = 0$ and $P = 60$. (a) $\mathrm{Re}(g_{L,60})$. (b) $\log_{10}|\mathrm{Re}(g_{L,60} - \hat{g}_{L,60})|$.

Subsequently, for each $\boldsymbol{r}^*$,

$$\langle \mathscr{L} g_{L,P}(\boldsymbol{r};\boldsymbol{r}^*), f(\boldsymbol{r})\rangle \to f(\boldsymbol{r}^*) \quad \text{as } P \to \infty \tag{22}$$

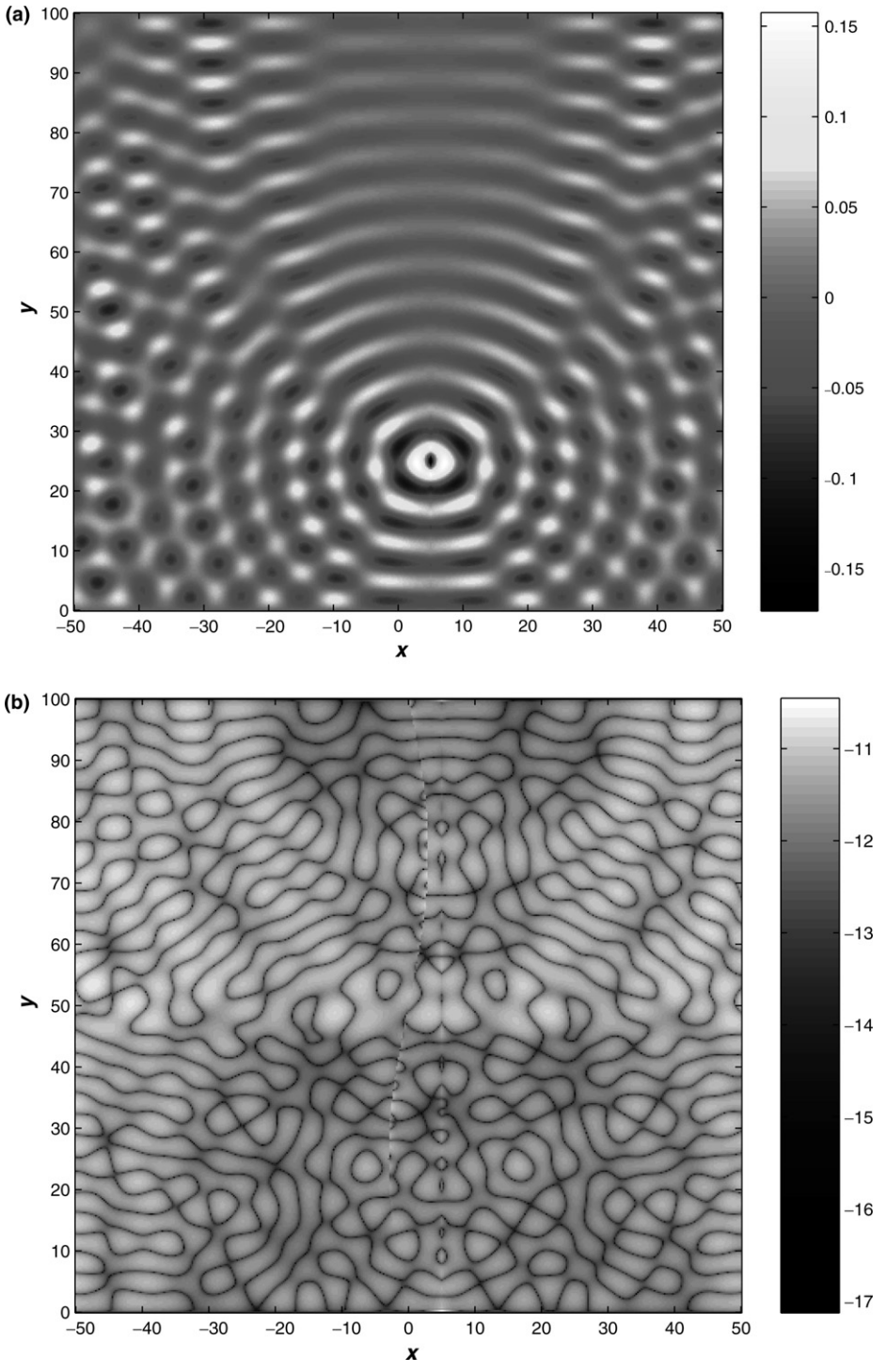

Fig. 3. Example 1: $E = 1$ and $P = 60$. (a) $\mathrm{Re}(g_{L,60})$. (b) $\log_{10}|\mathrm{Re}(g_{L,60} - \hat{g}_{L,60})|$.

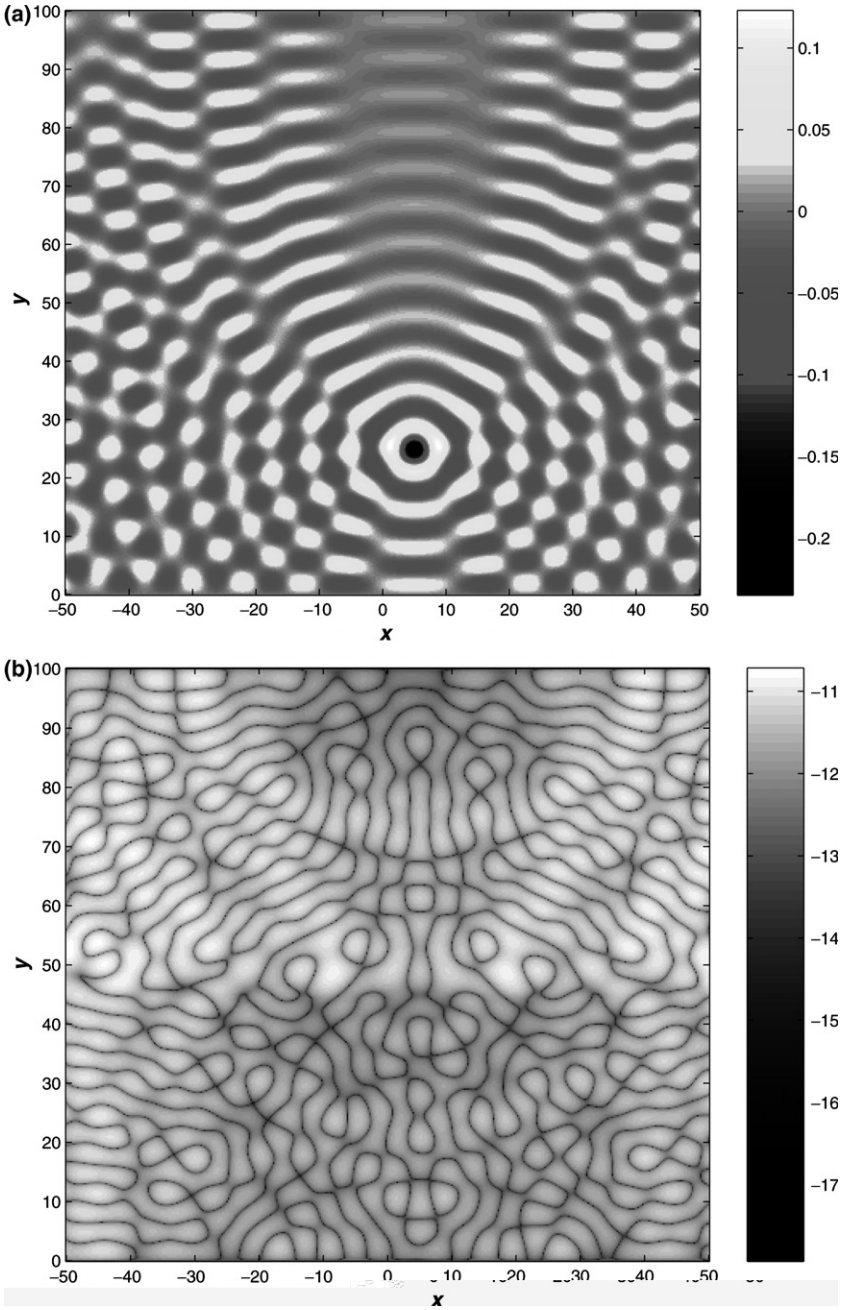

Fig. 4. Example 1: $E = 1$ and $P = 60$. (a) $\mathrm{Im}(g_{L,60})$. (b) $\log_{10}|\mathrm{Im}(g_{L,60} - \hat{g}_{L,60})|$.

Table 1
Example 1: errors in distribution

P	$E = 0$		$E = 1$	
	$f_P(\mathbf{r}^*)$	$\varepsilon_P(\mathbf{r}^*)$	$f_P(\mathbf{r}^*)$	$\varepsilon_P(\mathbf{r}^*)$
5	5.640	1.186e − 1	5.645 + 2.049e − 14i	1.243e − 1
10	5.525	3.825e − 3	5.531 + 9.554e − 15i	9.453e − 3
20	5.521	3.542e − 5	5.527 − 4.619e − 14i	5.589e − 3

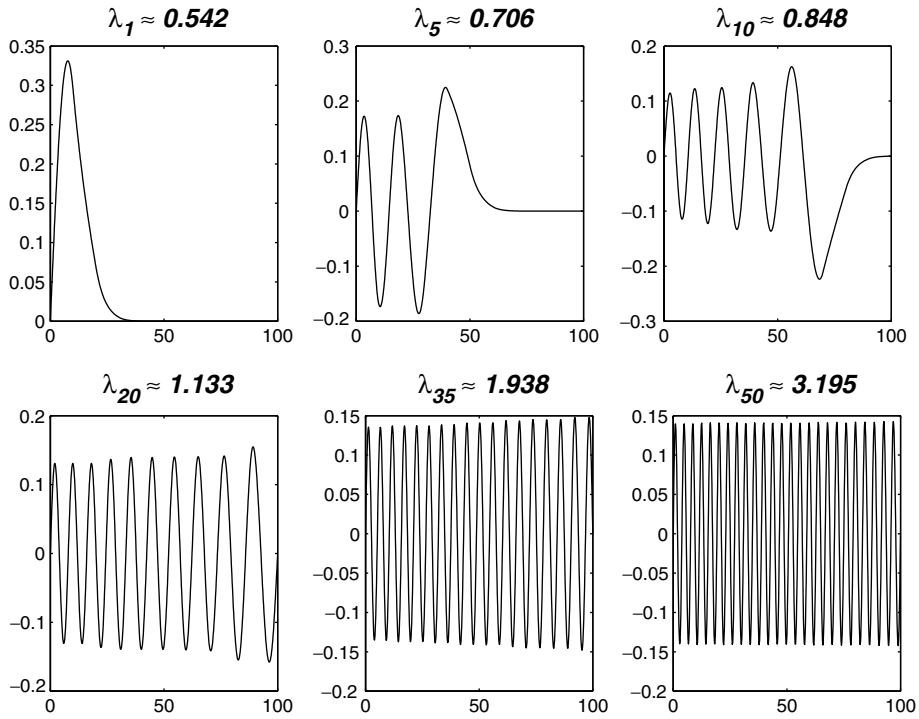

Fig. 5. Example 2: six calculated eigenfunctions.

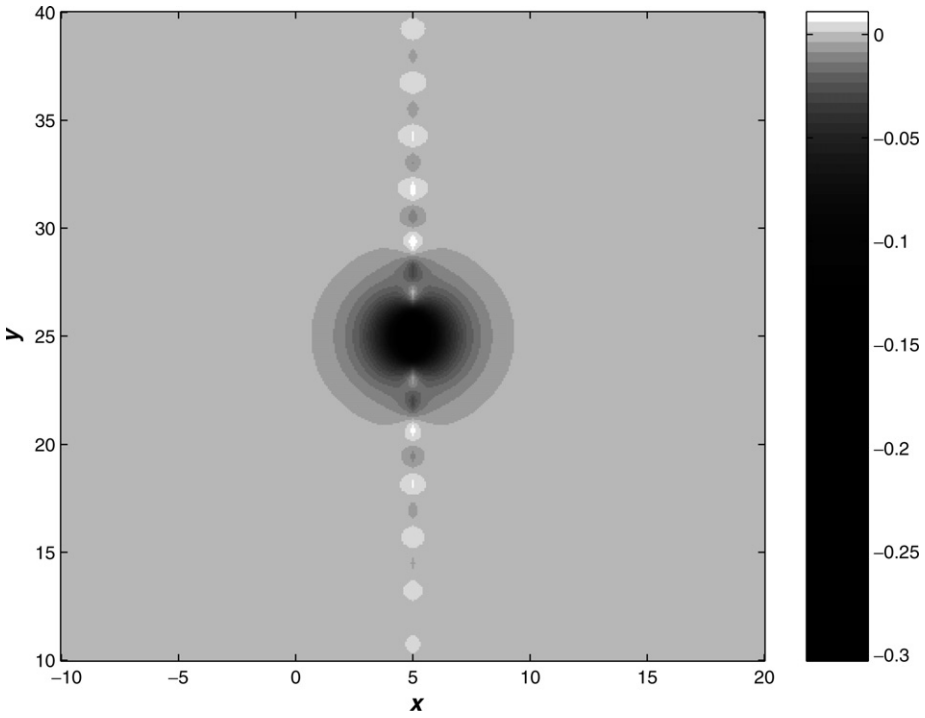

Fig. 6. Example 2: close-up of the real part of the Green's function, $\mathrm{Re}(g_{L,80})$, with $E = 0$ and $P = 80$.

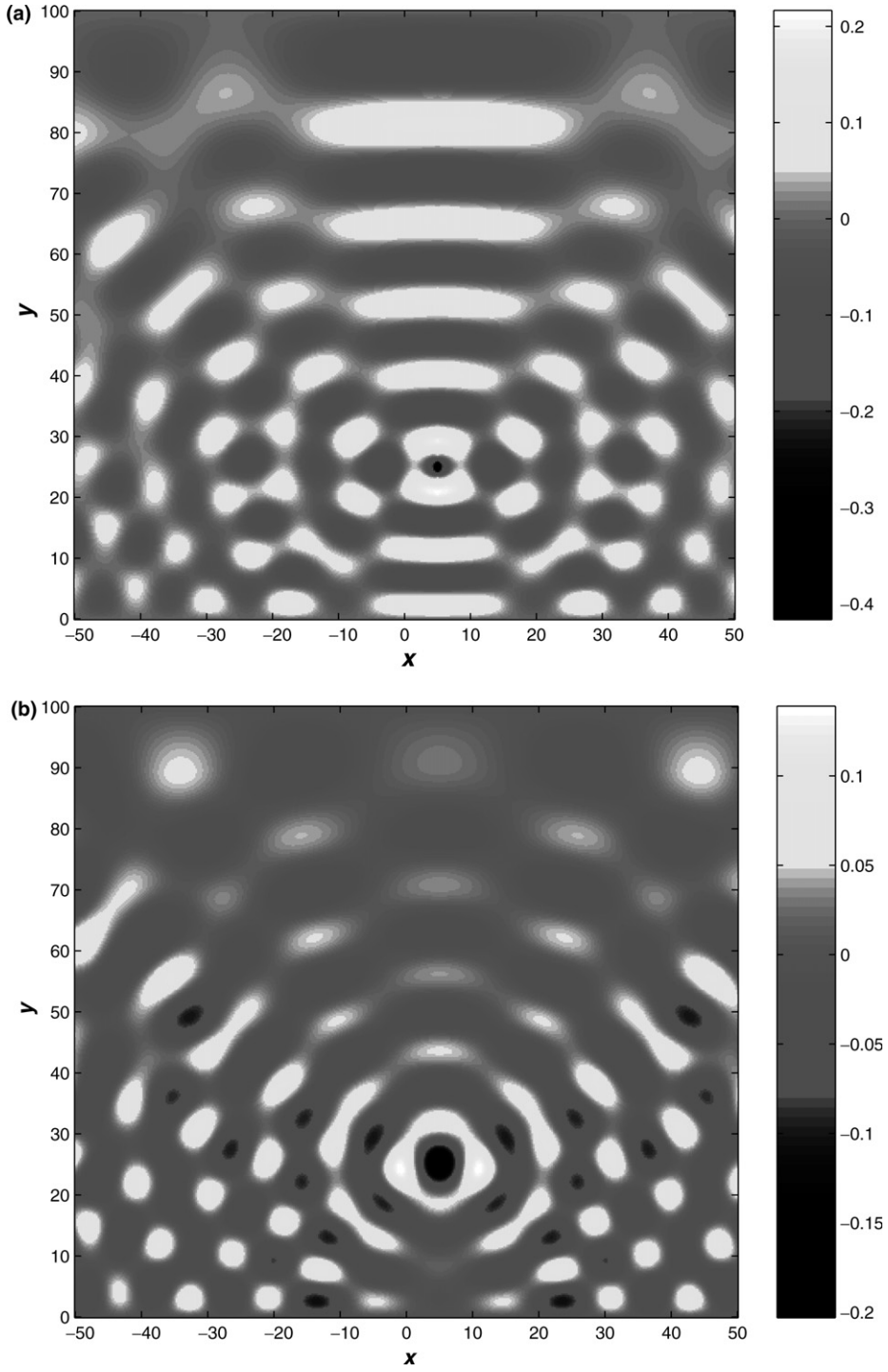

Fig. 7. Example 2: $E = 1$ and $P = 80$. (a) $\mathrm{Re}(g_{L,80})$. (b) $\mathrm{Im}(g_{L,80})$.

provided $f \in C_0^2(\Omega),\ \Omega \subset \Omega_L,\ \boldsymbol{r}^* \in \Omega$. $\langle \cdot,\cdot \rangle$ represents the inner product in L^2 space. Therefore, we define the error of the Green's function in the distribution sense as

$$\varepsilon_P(\boldsymbol{r}^*) = |f_P(\boldsymbol{r}^*) - f(\boldsymbol{r}^*)|, \tag{23}$$

where $f_P(\boldsymbol{r}^*) := \langle \mathscr{L} g_{L,P}(\boldsymbol{r}; \boldsymbol{r}^*), f(\boldsymbol{r}) \rangle$.

Table 2
Example 2: errors in distribution

P	$E=0$		$E=1$	
	$f_P(\boldsymbol{r}^*)$	$\varepsilon_P(\boldsymbol{r}^*)$	$f_P(\boldsymbol{r}^*)$	$\varepsilon_P(\boldsymbol{r}^*)$
10	6.085	5.642e−1	6.092 + 8.919e−10i	5.704e−1
20	5.528	6.675e−3	5.533 + 8.062e−7i	1.230e−2
40	5.520	7.872e−4	5.526 + 8.062e−7i	4.833e−3

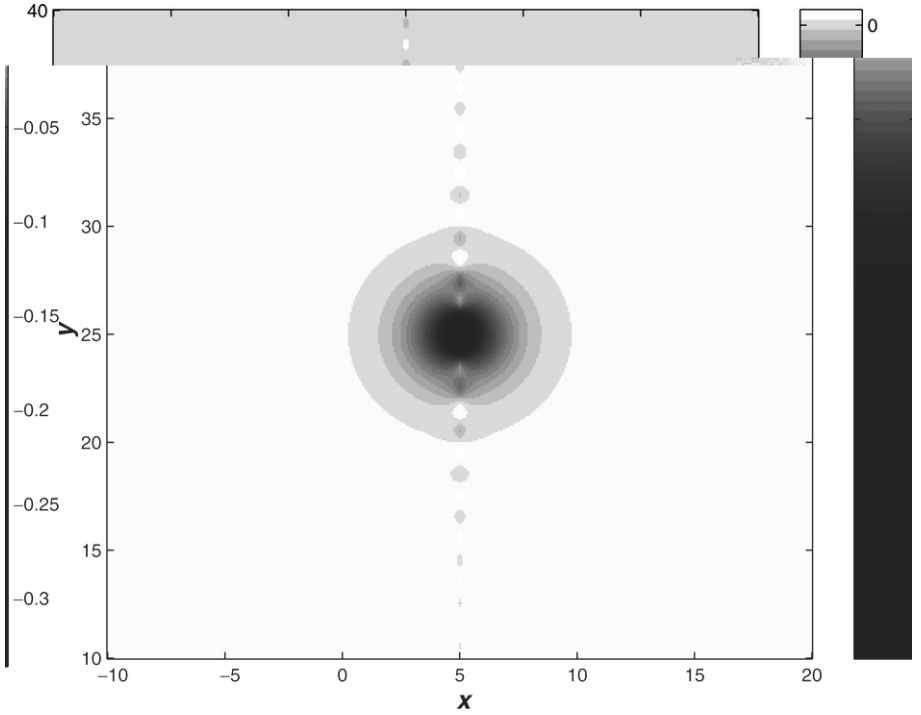

Fig. 8. Example 3: close-up of the real part of the Green's function, $\mathrm{Re}(g_{L,100})$, with $E=0$ and $P=100$.

In our numerical tests, we select $\Gamma_i=\{(x(t),y(t)):x(t)=-3\sin(2\pi t),\ y(t)=100t, t\in[0,1]\}$ and $\Omega=\{(x,y):-50\leqslant x\leqslant 50,\ 0\leqslant y\leqslant L=100\}$ which consists of N layers along y-direction, take $\hbar=1$, $m=0.5$, and

$$f(\boldsymbol{r})=1000\left(\left(\frac{x}{50}\right)^2-1\right)^3\left(\frac{y}{100}\right)^3\left(\frac{y}{100}-1\right)^3\sin\left[6\left(\frac{x}{50}+\frac{y}{100}\right)\right]$$

for error estimation. As an example, we take $\boldsymbol{r}^*=(5,25)$ where $f(\boldsymbol{r}^*)\equiv\frac{26198073}{4096000}\sin(\frac{21}{10})\simeq 5.521$. Moreover, we consider $N=10$ layers equally spaced vertically. In the Pruess method, the initial grid number in y-direction is 600 to ensure sufficient accuracy of the eigenfunctions.

Example 1. We consider the retarded Green's function for an infinite strip Ω_L, for which an analytic form can be obtained as follows:

$$\hat{g}_L(\boldsymbol{r};\boldsymbol{r}^*)=\sum_{p=1}^{\infty}-\frac{\mathrm{i}}{\hbar v_p}\psi_p(y)\psi_p(y^*)\exp(\mathrm{i}k_p|x-x^*|), \tag{24}$$

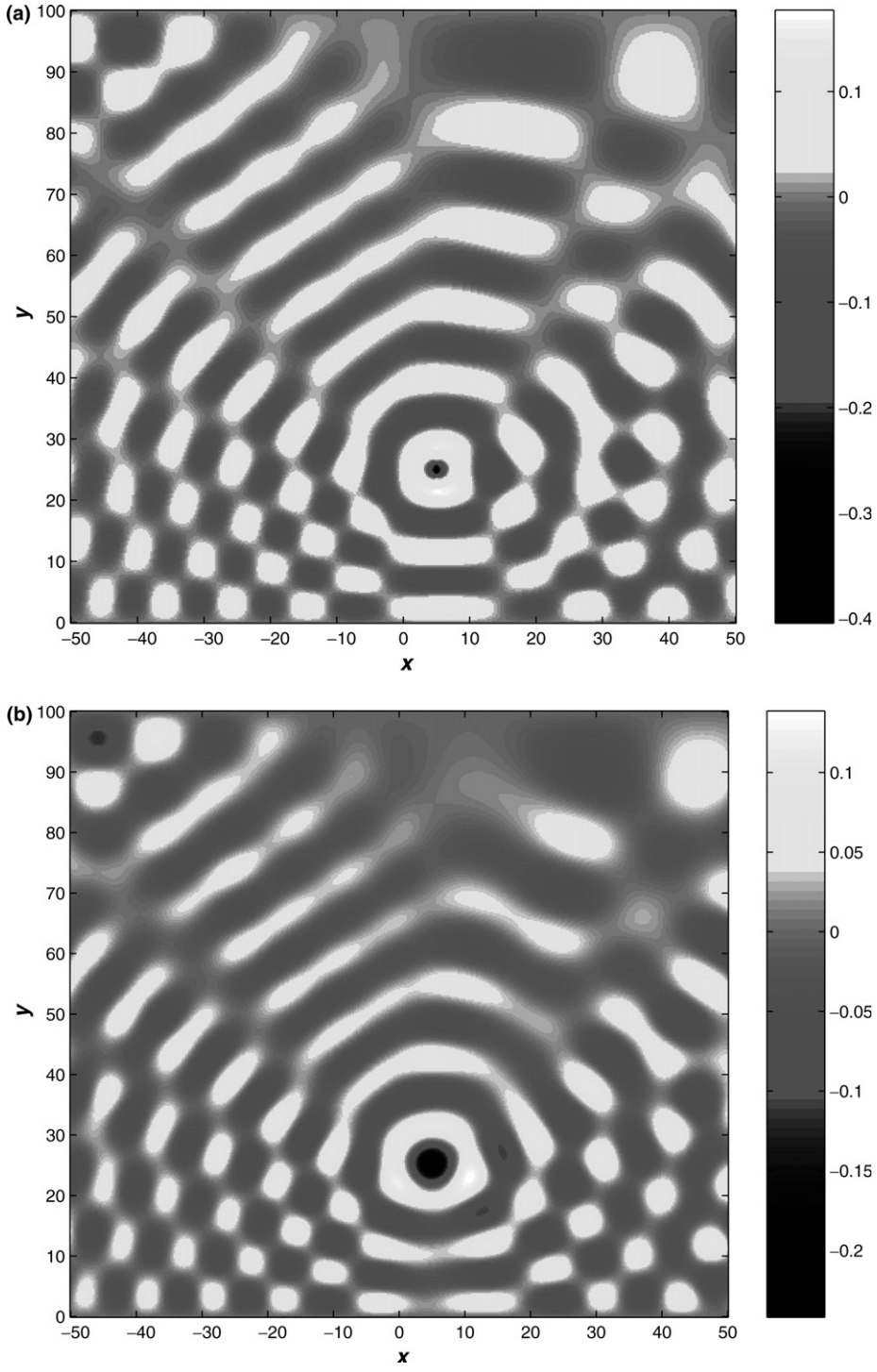

Fig. 9. Example 3: $E = 1$ and $P = 100$. (a) $\mathrm{Re}(g_{L,100})$. (b) $\mathrm{Im}(g_{L,100})$.

where $k_p = \frac{\sqrt{2m(E-\lambda_p)}}{\hbar}$, $v_p = \frac{\hbar k_p}{m}$ and $\psi_p(y)$, λ_p satisfy the equation

$$\left[\frac{\hbar^2}{2m}\frac{\mathrm{d}^2}{\mathrm{d}y^2} - V(y)\right]\psi_p(y) = -\lambda_p\psi_p(y), \quad 0 \leqslant y \leqslant L. \tag{25}$$

Table 3
Example 3: errors in distribution

P	$E=0$		$E=1$	
	$f_P(\boldsymbol{r}^*)$	$\varepsilon_P(\boldsymbol{r}^*)$	$f_P(\boldsymbol{r}^*)$	$\varepsilon_P(\boldsymbol{r}^*)$
20	5.554	3.323e−2	5.595 − 2.398e−2i	7.739e−2
30	5.517	3.830e−3	5.517 + 1.431e−5i	3.892e−3
40	5.521	3.127e−5	5.523 + 1.772e−4i	1.458e−3

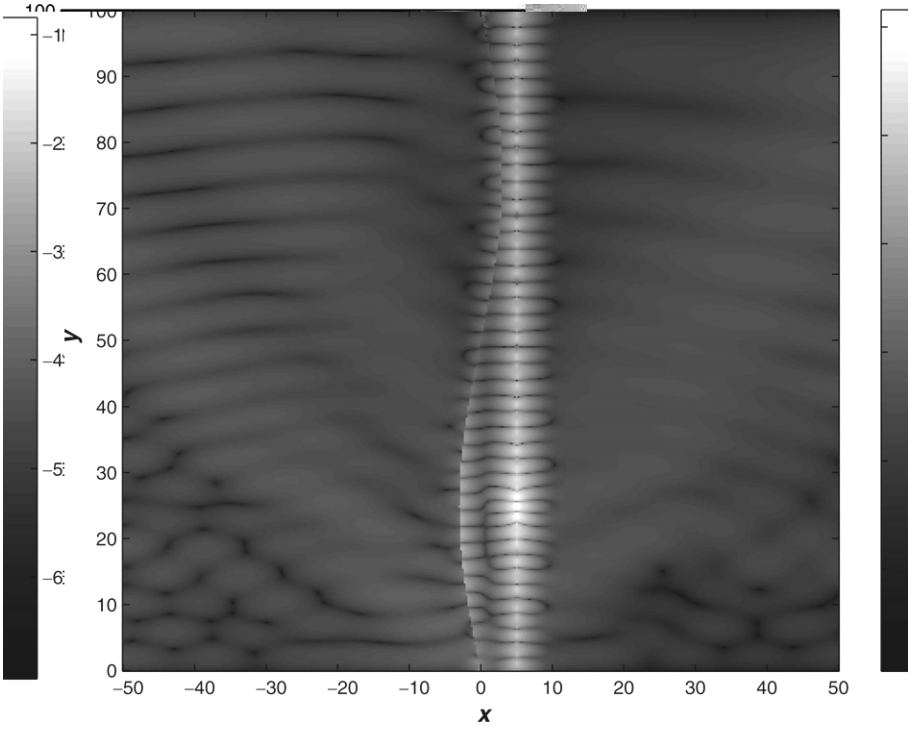

Fig. 10. Example 3: error $\log_{10}|g_{L,40} - g_{L,100}|$ with $E=1$.

The above Green's function $\hat{g}_L(\boldsymbol{r};\boldsymbol{r}^*)$ represents the wave function at $\boldsymbol{r}$ due to an excitation at $\boldsymbol{r}^*$ in an infinite wire, see [12].

To verify the accuracy of the algorithm, we set $V(y)\equiv 0$. Now the eigenvalues and eigenfunctions of (25) can be exactly derived as

$$\lambda_p = \left(\frac{p\pi}{L}\right)^2, \quad \psi_p(y) = \sqrt{\frac{2}{L}}\sin\frac{p\pi}{L}y. \tag{26}$$

Figs. 2–4 give plots of the Green's function $g_{L,P}(r;r^*)$ and the relative error $|g_{L,P}(\boldsymbol{r};\boldsymbol{r}^*) - \hat{g}_{L,P}(\boldsymbol{r};\boldsymbol{r}^*)|$ with truncation order $P=60$ in the domain $[-50,50]\times[0,100]$ for $E=0$ and 1, respectively. Here, $\hat{g}_{L,P}(\boldsymbol{r};\boldsymbol{r}^*)$ is the P-term series approximation of $\hat{g}_L(\boldsymbol{r};\boldsymbol{r}^*)$ in (24). When $E=0, \hat{g}_L$ is in fact the Green's function of the Poisson equation. The results show that the errors $|g_{L,P}(\boldsymbol{r};\boldsymbol{r}^*) - \hat{g}_{L,P}(\boldsymbol{r};\boldsymbol{r}^*)|$ are on the order of 10^{-10}. Thus, the truncations of the exact and numerical Green's function, $\hat{g}_{L,P}$ and $g_{L,P}$, are indistinguishable. On the other hand, the errors $\varepsilon_P(r^*)$ given in Table 1 show that the proposed algorithm is very accurate with respect to the truncation order P and has good convergence rate as the truncation parameter P is increased.

Example 2. In the second example, we take the potentials on two sides of the curved interface to consist of one single sequence of constant values, for instance, $V_k^{\mathrm{r}} = V_k^{\mathrm{l}} = 0.5 + 0.05(k-1),\ k=1,2,\ldots,N$.

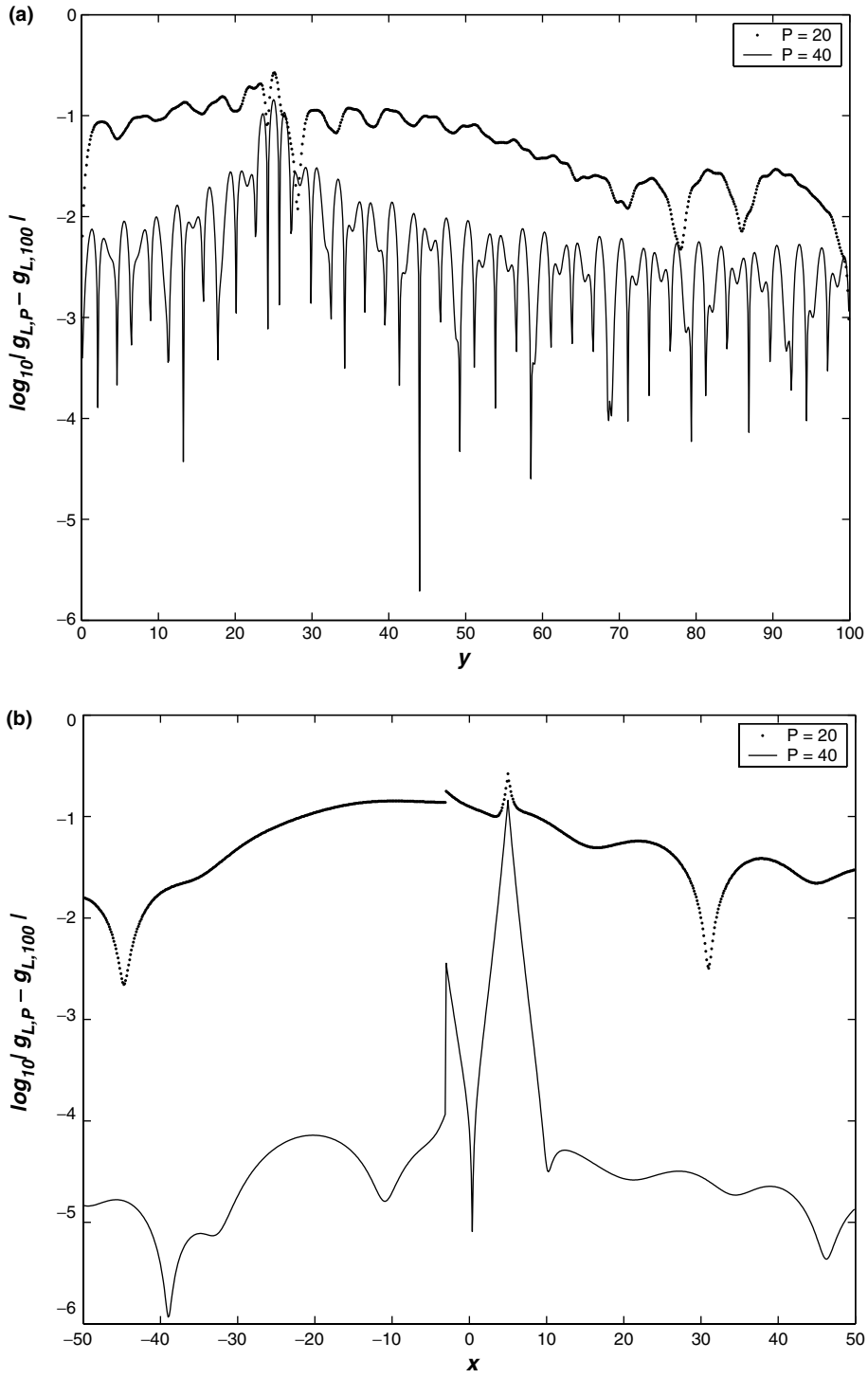

Fig. 11. Example 3: errors $\log_{10}|g_{L,P} - g_{\mathrm{L},100}|$ with $P = 20$ and 40 along two lines: (a) $x = x^*$; (b) $y = y^*$. $E = 1$.

In Fig. 5, we plot six eigenfunctions corresponding to the eigenvalues: λ_1, λ_5, λ_{10}, λ_{20}, λ_{35}, λ_{50}, obtained by the Pruess method. Figs. 6 and 7 plot the calculated Green's function $g_L(r; r^*)$ with truncation order $P = 80$ in the domain $[-50, 50] \times [0, 100]$ with $E = 0$ and 1, respectively. It can be seen that all computed

Green's functions have a symmetric profile with respect to the vertical line $x = x^*$. Table 2 gives the errors $\varepsilon_P(r^*)$. The results show that the proposed algorithm converges fast as the truncation parameter P is increased.

Example 3. The third example considered involves different potentials on two sides of the interface Γ_i: $V_k^r = 0.5 + 0.05(k-1), V_k^l = 0.4 + 0.04(k-1),\ k = 1, 2, \ldots, N$. Figs. 8 and 9 display the Green's function $g_L(r; r^*)$ with truncation order $P = 100$, calculated in the domain $[-50, 50] \times [0, 100]$ with $E = 0$ and 1, respectively. We see that the Green's function is not symmetric with respect to the vertical line $x = x^*$, the continuity conditions at Γ_i are satisfied nicely. The errors $\varepsilon_P(r^*)$ in Table 3 show that the proposed algorithm is again very accurate with respect to the truncation order P and has good convergence as the truncation parameter P is increased. We plot the error $\log_{10}|g_{L,40} - g_{L,100}|$ with $E = 1$ in Fig. 10, which shows that most of the large errors concentrate in the neighborhood of the singular point $r^* = (5, 25)$. In Fig. 11, we plot the errors $\log_{10}|g_{L,P} - g_{L,100}|$ with $P = 20$ and 40, along the line $x = x^* = 5$ and the line $y = y^* = 25$, respectively. Our algorithm gives good convergence away from the singular point of $g_L(r; r^*)$.

5. Conclusion

In this paper, we have introduced a novel numerical method for calculating the Green's function of the Schrödinger equation in a block layered potential based on eigenfunction expansions and a collocation matching procedure. Such a Green's function may also find applications in electromagnetic and sound wave scattering in block layered media. It should be mentioned that the method proposed in this paper can be extended to more than two column of blocks potentials or media. In principle, it can be generalized as an approximation algorithm for constructing Green's function of variable coefficient differential operators by using check-board type piecewise constant/piecewise linear approximation of the coefficients.

Acknowledgments

Wei Cai thanks the support of the National Science Foundation (Grant Nos. DMS-0408309, CCF-0513179) and Department of Energy (Grant No. DEFG0205ER25678) and NERSC Computing Award for the work reported in this paper. Support from the Department of Mathematics at Hong Kong Baptist University is also acknowledged for a sabbatical visit in 2005, during which the work on this paper is initiated. Huazhong Tang thanks for partial support of the National Basic Research Program under the Grant 2005CB321703 and the National Natural Science Foundation of China (Grant No. 10431050).

Appendix A. Pruess algorithm

Consider a general Sturm–Liouville problem

$$\begin{aligned} &-\frac{\mathrm{d}}{\mathrm{d}x}\left(r(x)\frac{\mathrm{d}u}{\mathrm{d}x}\right) + s(x)u = \lambda t(x)u, \\ &a_1 u(a) = a_2 r(a)u'(a), \quad b_1 u(b) = b_2 r(b)u'(b). \end{aligned} \tag{A.1}$$

In the Pruss method, an approximated Sturm–Liouville problem for the above

$$\begin{aligned} &-\frac{\mathrm{d}}{\mathrm{d}x}\left(R(x)\frac{\mathrm{d}U}{\mathrm{d}x}\right) + S(x)U = \Lambda T(x)U, \\ &a_1 U(a) = a_2 R(a)U'(a), \quad b_1 U(b) = b_2 R(b)U'(b) \end{aligned}$$

is numerically solved. Here, $R(x)$, $S(x)$ and $T(x)$ are piecewise constant approximations of functions $r(x)$, $s(x)$ and $t(x)$ in (A.1). Given a mesh $a = x_0 < x_1, \ldots, x_{N-1} < x_N = b$, and define $x_{i-\frac{1}{2}} = (x_{i-1} + x_i)/2$. Then, $R(x)$, $S(x)$ and $T(x)$ are defined by

$$R(x) = r(x_{i-\frac{1}{2}}) := r_i, \quad S(x) = s(x_{i-\frac{1}{2}}) := s_i, \quad T(x) = t(x_{i-\frac{1}{2}}) := t_i,$$

$x \in (x_{i-1}, x_i)$ for all $1 \leqslant i \leqslant N$. An "explicit" solution of (5) is easily derived as follows:

$$U(x) = U_{i-1}\Phi_i'(x - x_{i-1}) + (RU')_{i-1}\Phi_i(x - x_{i-1})/r_i, \quad x \in [x_{i-1}, x_i], \tag{A.2}$$

where $U_i = U(x_i)$, $(RU')_i = (RU')(x_i)$, and

$$\Phi_i(\tau) = \begin{cases} \sin(\omega_i\tau)/\omega_i, & k_i > 0, \\ \tau, & k_i = 0, \\ \sinh(\omega_i\tau)/\omega_i, & k_i < 0. \end{cases} \tag{A.3}$$

Here $k_i = \frac{\Delta t_i - s_i}{r_i}$ and $\omega_i = \sqrt{|k_i|}$. Then, setting $x = x_i$ in (A.2) gives

$$\begin{pmatrix} (RU')_i \\ U_i \end{pmatrix} = O_i \begin{pmatrix} (RU')_{i-1} \\ U_{i-1} \end{pmatrix}, \quad O_i = \begin{pmatrix} r_i\Phi_i' & r_i\Phi_i'' \\ \Phi_i & \Phi_i' \end{pmatrix}(x_i - x_{i-1}), \tag{A.4}$$

subject to initial data

$$\begin{pmatrix} (RU')_0 \\ U_0 \end{pmatrix} = \begin{pmatrix} a_1 \\ a_2 \end{pmatrix} \quad \text{and} \quad \begin{pmatrix} (RU')_N \\ U_N \end{pmatrix} = \begin{pmatrix} b_1 \\ b_2 \end{pmatrix}.$$

Finally, we can use a shooting method to find the eigenvalues and eigenfunctions of the approximating problem (5). We refer the readers to [10,11] for a detailed description of Pruess method.

References

[1] A. Taflove, S.C. Hagness, Computational Electromagnetics: The Finite-Difference Time-Domain Method, second ed., Artech House, Boston/London, 2000.
[2] J.M. Jin, The Finite Element Method in Electromagnetics, Wiley, New York, 2002.
[3] T. Lu, P.W. Zhang, W. Cai, Discontinuous Galerkin methods for dispersive and lossy Maxwell's equations, J. Comput. Phys. 200 (2004) 549–580.
[4] K.A. Michalski, D. Zheng, Electromagnetic scattering and radiation by surfaces of arbitrary shape in layered media, Part I and Part II, IEEE Trans. Antennas Propag. 38 (1990) 335–352.
[5] W.C. Chew, Response of a source on top of a vertically stratified half-space, IEEE Trans. Antennas Propag. AP-33 (1985) 649–654.
[6] Q.H. Liu, W.C. Chew, Numerical mode-matching method for the multi-region vertically stratified media, IEEE Trans. Antennas Propag. 38 (1990) 498–506.
[7] W. Cai, T.J. Yu, Fast calculation of dyadic Green's functions for electromagnetic scattering in a multi-layered medium, J. Comput. Phys. 165 (2000) 1–21.
[8] D. Ferry, S.M. Goodnick, Transport in Nanostructures, Cambridge University Press, Cambridge, 1997.
[9] N. Dunford, J. Schwartz, Linear Operators, Part II, Interscience, New York, 1963.
[10] J.D. Pryce, Numerical Solution of Sturm–Liouville Problems, Oxford University Press, New York, 1993.
[11] S. Pruess, C.T. Fulton, Mathematical software for Sturm–Liouville problems, ACM Trans. Math. Software 19 (1993) 360–376.
[12] S. Datta, Electronic Transport in Mesoscopic Systems, Cambridge University Press, Cambridge, 1995.